Tourmaline as a petrogenetic indicator highlighted in a multicoloured crystal from the gem deposit of Mavuco (Alto Ligoña pegmatite district, NE Mozambique)

Alessandra Altieri[1*], Federico Pezzotta[2], Henrik Skogby[3], Ulf Hålenius[3], Ferdinando Bosi[1,4]

[1] Department of Earth Sciences, Sapienza University of Rome, Piazzale Aldo Moro 5, I-00185 Rome, Italy

[2] MUM – Mineralogical Museum "Luigi Celleri", San Piero in Campo, Elba Island, Italy

[3] Department of Geosciences, Swedish Museum of Natural History, Box 50007, SE-10405 Stockholm, Sweden

[4] CNR-IGAG c/o Department of Earth Sciences, Sapienza University of Rome, Italy

*Corresponding author: alessandra.altieri@uniroma1.it

Abstract

A rounded fragment of a multicoloured tourmaline crystal of sizes up to 2.5 cm, collected from the secondary gem deposit of Mavuco (Alto Ligoña pegmatite district, Mozambique), has been investigated using a multi-analytical approach, with the goal of reconstructing its growth history. The sample represents a core-to-rim section, perpendicular to the **c**-axis, of a crystal characterised by a variety of colours. The colours change from a black core to an intermediate zone with a series of colours such as yellow, blue-green, and purple, to a final dark-green prismatic overgrowth. This change is the result of a wide variation in Fe, Mn, Ti, and Cu concentrations and their redox state. The black core is characterised by an enrichment in Fe and Mn, with iron present in its divalent state. The yellow zone shows a progressive depletion in Fe and its coloration is caused by Mn^{2+} and

This is a 'preproof' accepted article for Mineralogical Magazine. This version may be subject to change during the production process.
DOI: 10.1180/mgm.2024.42

Mn^{2+}-Ti^{4+} IVCT interactions. The progressive decrease in Mn coupled with the absence of Ti, and the lack of Fe, allow Cu^{2+} to act as the only chromophore in the pale blue-green zone. The dominant colour-causing agent of the purplish zone is Mn^{3+}, denoting a change in redox environment; however, despite the amount of Cu remains significant, its chromophore effect is obscured by Mn^{3+}. The dark-green prismatic overgrowth, characterized by a sharp increase in Fe, Mn and also Ca, is interpreted as a late-stage partial re-opening of the geochemical system. This occurrence could potentially be related to mechanical instability of the cavity in which the crystal grew.

Keywords: tourmaline-supergroup minerals, petrogenetic indicator, growth history, gem-tourmaline, Paraiba tourmaline, cuprian tourmaline, electron microprobe, optical absorption spectroscopy, Mössbauer spectroscopy.

1. Introduction

Tourmaline is the dominant host for boron in most rocks of the Earth's crust. It occurs in granites and granitic pegmatites, but also in sedimentary and in low-grade to ultrahigh-pressure metamorphic rocks and as detrital grains in sandstones and conglomerates (Ertl et al., 2010; van Hinsberg et al., 2011a,b; Dutrow and Henry, 2018; Henry and Dutrow, 2018). Tourmaline-supergroup minerals are complex borosilicates with a significant chemical variability containing both light and heavy elements, from H to Pb, and across multiple valence states. This variability results in a wide range of distinct mineral species. The general chemical formula of tourmaline-supergroup minerals can be written as $XY_3Z_6T_6O_{18}(BO_3)_3V_3W$, where X = Na, K, Ca, Pb, □ (□ = vacancy); Y = Al, Fe^{3+}, Mn^{3+}, Cr, V, Mg, Fe^{2+}, Mn^{2+}, Li, Ti; Z = Al, Fe, Cr, V, Mg, Fe^{2+}; T = Si, Al, B; B = B^{3+}; V = (OH), O and W = (OH), F, O (Henry et al., 2011). The non-italicized letters X, Y, Z, T and B represent groups of cations accommodated at the $^{[9]}X$, $^{[6]}Y$, $^{[6]}Z$, $^{[4]}T$ and $^{[3]}B$ crystallographic sites (italicized letters). The letters V and W represent groups of anions accommodated at the $^{[3]}O(3)$ and $^{[3]}O(1)$ crystallographic sites, respectively. The H atoms occupy

https://doi.org/10.1180/mgm.2024.42 Published online by Cambridge University Press

the H(3) and H(1) sites, which are related to O(3) and O(1), respectively.

According to the dominance of specific ions at one or more sites of the crystal structure, the tourmaline-supergroup minerals can be classified in three primary groups based on the *X*-site occupancy: *X*-site vacant, alkali and calcic (Henry et al., 2011). A further level of classification into subgroups is based on charge arrangements at the *Y* and *Z* sites. Tourmalines are also distinguished by the dominant W anion into hydroxy-, fluor- and oxy-species (Henry et al., 2011). In particular, occupancy of the *X* and *Y*-site is useful to reconstruct the chemical history of the fluids involved in tourmaline crystallization (van Hinsberg et al., 2011a,b; Dutrow and Henry, 2018; Bosi et al., 2022; Altieri et al., 2022; 2023a,b).

Tourmaline is well known to be an efficient geological tool for investigating *P–T–X* conditions in all crustal settings within the Earth given its ability to register and preserve the chemical composition and the redox conditions of the environment in which it crystallised (Dutrow and Henry, 2011). Colour-zoning in tourmaline generally highlights internal variations in composition, which reflects an evolution in the physico-chemical characteristics of the pegmatitic fluid during its crystallisation (e.g., Dutrow and Henry, 2018; Altieri et al., 2022; 2023a,b).

The Mavuco tourmaline gem deposit, located in the Alto Ligoña pegmatite district (NE Mozambique), is internationally known to be the source of a quantity of very valuable Cu-bearing gem tourmalines also known as "Paraiba" variety (Laurs et al., 2008; Ertl et al., 2013; Okrusch et al., 2016). Nevertheless, since the deposit is of secondary origin, very little is known about the original primary deposit in which the tourmalines formed. In order to investigate the nature of the primary deposit and eventual changes in the crystallisation environment, and thus to reconstruct the tourmaline growth history, a tourmaline sample composed by a large fragment of a multicolour crystal, has been chosen to represent, as far as possible, the variety of colours occurring in the deposit. This multicoloured sample has been subject to an in-depth analysis using a multi-analytical approach, which included electron microprobe analysis, optical absorption and Mössbauer spectroscopic investigations.

https://doi.org/10.1180/mgm.2024.42 Published online by Cambridge University Press

1.1 Sample occurrence

The mining area of Mavuco consists of a secondary deposit of over 12 km^2 located in the Alto Ligoña pegmatite district, in NE Mozambique (Figure 1a). In this secondary deposit, tourmalines occur as fragments, ranging usually from 1g to over 100g of sub-angular to sub-rounded shapes, inside a residual level of the soil mostly composed of quartz fragments, occasionally associated with fragments of beryl gem varieties and spessartine, called by local miners *kamada*, with a thickness ranging from a few cm up to 1 m. The *kamada* layer occurs on top of the altered bed rock, which is in general composed of amphibolitic paragneiss, and more rarely of marble lenses, and aplitic and pegmatitic veins. A reddish-brownish soil unit, with a thickness from 1 m up to exceptionally over 10 m, of bauxitic nature more or less rich in iron hydroxides nodules and with sparse small quartz grains and no tourmaline and other gemstones, sits on top of the *kamada* and it is named by local miners *kororo*.

This secondary gem deposit was interpreted by Laurs et al. (2008) (Figure 1b) as of alluvial origin, with the primary pegmatitic tourmaline deposits eroded and transported by the seasonal streams through spasmodic flash floods downhill to the Mavuco area where they were deposited (Laurs et al., 2008). Nevertheless, the systematic observations made by one of the authors (FP) of the soil sections exposed during the mechanized excavations for the mining of gem tourmalines, performed by the Mozambique Gems company, are showing that the distribution and the thickness of the *kamada* are not related to the morphology and hydrology of the land, and indeed the *kamada* represents a very persistent unit in the soil occurring at various depth, place to place, always at the top of the altered unit of the bed-rock. Moreover, the occurrence in the *kamada* of quartz and tourmaline clasts, and occasionally beryl and spessartine clasts, which still preserve quite well-defined crystal faces, together with clasts which are partially rounded to very rounded, and the local increase of the *kamada* thickness at the intersection and in the surrounding areas of altered quartz and pegmatitic veins still observable in the altered bedrock, are elements in favour of a eluvial and

https://doi.org/10.1180/mgm.2024.42 Published online by Cambridge University Press

locally colluvial origin of such soil unit; thus, the minerals found as fragments in the *kamada* are the result of an in situ erosion of a primary deposit, composed very likely by a series of pegmatitic veins, which, at least in part, still exist at depth. Further studies are in progress by the previously mentioned author to better define this genetic model of the deposit.

2. Materials and methods

2.1 Sample

A sample consisting of a large fragment (2.5-cm diameter, 12.75-gr weight) of a multicoloured tourmaline crystal collected from the secondary deposit of Mavuco, roughly representative of a core to rim section perpendicular to the **c**-axis, was chosen for the present study (Figure 2, left). The sample displays a sub-rounded shape originated by the natural breaking and erosion of an original prismatic crystal, characterized by a black core, an intermediate polychromatic zone (yellow, pale blue-green, purple) and a dark-coloured rim.

On the basis of the chemical and colour inhomogeneity, the sample was divided in different zones. The area corresponding to the core zone, the intermediate polychromatic zone and the dark-green prismatic rim were labelled "C", "I" and "R", respectively. The "I" and "C" zones were further subdivided, in presence of changes in composition or colour, by adding a progressive numerical suffix starting from the core of the crystal.

2.2 Sample preparation

The tourmaline sample was glued to a glass-slide using epoxy resin. Then, a crystal slice was cut and subsequently ground and polished to produce a flat surface with a uniform thickness of 500 µm for chemical microanalysis (Figure 2, right).

For optical absorption spectroscopy analysis, crystal slices cut from the different coloured zones were glued to a glass-slide using a thermoplastic resin. Before analysis, each coloured slice was further thinned to appropriate thickness (yellow intermediate zone: 280 µm; pale blue-green

https://doi.org/10.1180/mgm.2024.42 Published online by Cambridge University Press

intermediate zone: 838 μm; purple intermediate zone: 843 μm; dark-green rim: 424 μm) and doubly polished.

2.3 Electron Microprobe analysis (EMPA)

Compositional data of the tourmaline sample was collected along a straight traverse from the black core to the dark-green rim with an average step size of 500 μm, using a CAMECA SX50 electron-microprobe at the Istituto di Geologia Ambientale e Geoingegneria (CNR of Rome, Italy). A total of 44 spot analyses were obtained. EMP analyses were done operating in Wavelength-Dispersion-Spectroscopy mode with an accelerating potential of 15 kV, a sample current of 15 nA and a beam diameter of 10 μm. Minerals and synthetic compounds were used as reference materials: wollastonite (Si, Ca), magnetite (Fe), rutile (Ti), corundum (Al), karelianite (V), fluorphlogopite (F), periclase (Mg), jadeite (Na), orthoclase (K), rhodonite (Mn) and metallic Cr, Cu and Zn. The PAP correction procedure for quantitative electron probe micro analysis was applied (Pouchou and Pichoir, 1991). Relative error on data was < 1% and detection limits < 0.03 wt%.

2.4 Mössbauer spectroscopy (MS)

^{57}Fe Mössbauer spectra of the Fe-rich colored zones of the analyzed tourmaline sample were collected using a conventional spectrometer system equipped with a 50 mCi source and operated in constant acceleration mode. The absorbers were prepared from 60 to 135 mg ground sample material that was mixed with an acrylic resin and pressed to 12-mm diameter discs under mild heating (<150°C). Data were collected at room temperature over the velocity range ± 4.2 mm/s and recorded in a multichannel analyser with 1024 channels. The velocity was calibrated with an α-Fe foil. The obtained spectra were fitted using unconstrained Lorentzian doublets with the aid of the sofware MossA (Prescher et al., 2012).

2.5 Optical absorption spectroscopy (OAS)

https://doi.org/10.1180/mgm.2024.42 Published online by Cambridge University Press

Unpolarized, room temperature optical absorption spectra of the polychromatic core zone and the dark-green rim, in the range of 30500–11000 cm^{-1}, were obtained at a spectral resolution of 1 nm on doubly polished sections, using an AVASPEC-ULS2048 × 16 spectrometer attached via a 400 µm ultraviolet (UV) optical fibre cable to a Zeiss Axiotron UV-microscope. A 75 W Xenon arc lamp was used as light source and Zeiss Ultrafluar 10× lenses served as objective and condenser. Data in the NIR region (11000–5000 cm^{-1}) were measured using a Bruker Vertex 70 spectrometer attached to a Hyperion 2000 microscope and equipped with a halogen lamp source, a CaF_2 beamsplitter and an InSb detector at resolution of 4 cm^{-1}.

2.6 Determination of atomic fractions

The wt% of element oxides determined by EMPA (Table 1) was used to calculate the atomic fractions (atoms per formula unit, apfu). The B content was assumed to be stoichiometric (B = 3.00 apfu). Lithium was calculated in accord with Pesquera et al. (2016). Iron oxidation state in the Fe-rich coloured zones was determined by MS (Table 2). The (OH) content was calculated by charge balance with the assumption of (T + Y + Z) = 15.00 apfu and 31 anions. The site populations and the empirical formulae (Table 3) of the different coloured zones of the analyzed tourmaline sample were calculated following the site allocation of ions recommended by Henry et al. (2011).

3. Results

3.1 Chemical composition

Electron microprobe analyses of the sample revealed a wide variation in Fe- and Mn-concentrations, which results in marked changes in colour from the black core, to yellow, pale blue-green, purple in the intermediate zone, and to dark-green at the prismatic overgrowth, representing the rim. Calcium, Ti, Cu and F are also characterised by some variation along the traverse. Vanadium, Cr and Zn were below detection limits.

https://doi.org/10.1180/mgm.2024.42 Published online by Cambridge University Press

Figure 3 displays the pattern of selected elements (as wt% oxides) determined along the considered traverse. Table 1 summarizes the average chemical compositions for each coloured zone.

The black core of the sample (C1 and C2) is characterized by a high enrichment in Fe and Mn (FeO ~5 wt% and MnO ~4 wt%), which remains quite constant throughout the section (Figure 3). Within the intermediate polychromatic zone, the yellow one (I1) shows a sharp increase in MnO, reaching values up to 7 wt%, and a simultaneous drop of FeO to values below 1 wt% (Figure 3). A decrease in the concentration of MnO occurs in the pale blue-green zone (I2), with a progressively decrease to below 1 wt% approaching the end of the purple zone (I3), as well as FeO, which content reaches values below detection in the I3 zone (Figure 3). The dark-green prismatic rim (R) is characterized by a sharp increase in FeO and a moderate increase in MnO concentration, reaching values up to 1.4 and 1.2 wt%, respectively (Figure 3).

Besides FeO and MnO, also CuO, TiO_2 and CaO, show significant changes within the crystal. CuO concentration is above detection only in the yellow I1 zone, in the pale blue-green I2 zone and in the purple I3 zone, with values up to 0.15 wt% (Figure 3). Titanium is mostly concentrated in the C1, C2 and I1 zones, with values of TiO_2 ranging from 0.45 to 0.65 wt%, while is below 0.05 wt% in the I2 and I3 zones and the dark-green prismatic overgrowth (Table 1). A peculiar behaviour is followed by CaO content, which is normally low across all the zones of the crystal, but displays an abrupt increase in the R zone, reaching values of ~4 wt% (Figure 3).

3.2 MS data and iron speciation

Portions of the black core (C1, C2), the yellow intermediate zone (I1) and the dark-green prismatic overgrowth (R), characterized by a significant Fe content, were subjected to MS analysis to evaluate the Fe oxidation state and its amount. The hyperfine parameters of the MS doublets and the relative Fe oxidation state and site assignment for each sample analyzed are summarized in Table 2. The spectrum of the black core zone was fitted with four doubles. The first three doublets are

https://doi.org/10.1180/mgm.2024.42 Published online by Cambridge University Press

compatible with Fe^{2+} occurring at the *Y*-site (Andreozzi et al., 2008). However, a unique Fe site-distribution cannot be achieved due to the limited resolution of the absorption doublets. A fourth weak doublet (3.2%) was interpreted as $Fe^{2.5+}$ due to electron delocalization. This resulted in a $Fe^{3+}/\Sigma Fe_{tot}$-ratio of 0.02 (with $Fe^{2.5+}$ distributed equally on Fe^{2+} and Fe^{3+}), suggesting that Fe^{2+} is strongly dominating in the black core zone of the sample (Figure 4a). The spectrum of the yellow intermediate zone has been fitted with only Fe^{2+} doublets compatible with *Y* site occupancy, without any indication of Fe^{3+} (Figure 4b). For the dark-green overgrowth, a model with four absorption doublets was adopted. The first three doublets were interpreted as Fe^{2+} at the *Y* site (*Y*1, *Y*2 and *Y*3), while the fourth doublet is consistent with Fe^{3+} (4% of Fe_{tot}) (Figure 4c).

3.3 Optical spectra

As stated above, the studied tourmaline sample is characterized by a marked polychroism. Thus, the different coloured zones were subjected to optical absorption spectroscopy analysis in the UV-Vis region. Spectra of the yellow, pale blue-green and purple intermediate zones and the dark-green prismatic overgrowth are reported in Figure 5.

The spectrum of the yellow intermediate zone (I1) shows a very strong absorption band in the near UV-region at ~30700 cm^{-1} and a sharp and very weak absorption band at ~24000 cm^{-1}. The spectrum recorded in the pale blue-green intermediate zone (I2) reveals only the presence of a very weak broad band at ~14000 cm^{-1} and an intense broad band at ~11000 cm^{-1} in the near-infrared-range. The recorded optical absorption spectrum of the purple intermediate zone (I3) is characterized by weak and broad absorption bands at ~25200 cm^{-1}, ~22000 cm^{-1} and ~14000 cm^{-1}, and a stronger broad band at ~19000 cm^{-1}. The spectrum of dark-green prismatic overgrowth displays two broad absorption bands centred at 13800 cm^{-1} and 9200 cm^{-1}, and a set of weak and relatively sharp bands between ~25000−24000 cm^{-1}.

The set of sharp bands, in the NIR region of spectra between 6700–7200 cm^{-1}, are due to overtones of the fundamental (OH)-stretching modes. These bands are obscured in the spectrum of

https://doi.org/10.1180/mgm.2024.42 Published online by Cambridge University Press

the dark-green overgrowth by the strong absorption band at ~9000 cm^{-1}, and barely visible in the spectrum of the yellow intermediate zone (I1) due to the reduced thickness.

3.4 Classification of tourmaline species in the multicoloured crystal from the gem deposit of Mavuco, Alto Ligoña pegmatite district, Mozambique

The empirical formulae (Table 3) show that the composition of the black core zone (C1), as well as the yellow (I1), the pale blue-green (I2) and the purple (I3) intermediate zones, are consistent with a tourmaline belonging to the alkali-group, subgroup 2 (Henry et al., 2011): they are Na-dominant at the X position of the tourmaline general formula and fluor-dominant at W with $(OH+F)^{-} > O^{2-}$ and F >> (OH). In addition, they are ^{Z}Al- and $^{Y}(Al_{1.5}Li_{1.5})$-dominant. Thus, the black core zone (C1), the yellow (I1), the pale blue-green (I2) and the purple (I3) intermediate zones can be classified as fluor-elbaite, ideally $Na(Li_{1.5}Al_{1.5})Al_6Si_6O_{18}(BO_3)_3(OH)_3F$.

The outer part of the black core (C2) can be, instead, classified as a tourmaline belonging to the alkali-group, subgroup 4 (Henry et al., 2011): it is Na-dominant at the X position of the tourmaline general formula and oxy-dominant at W with $O^{2-} > F^{-}$. Because is ^{Z}Al- and $^{Y}(Al_2Li)$-dominant, its composition can be ascribed to a darrellhenryite, ideally $Na(Al_2Li)Al_6(Si_6O_{18})(BO_3)_3(OH)_3O$.

In contrast, the dark-green prismatic rim (R) can be classified as a tourmaline belonging to the calcic-group, subgroup 2 (Henry et al., 2011): it is Ca-dominant at the X position and fluor-dominant at W with $(OH+F)^{-} > O^{2-}$ and F >> (OH). Because it is ^{Z}Al- and $^{Y}(Li_2Al)$-dominant, its composition can be ascribed to a fluor-liddicoatite, ideally $Ca(Li_2Al)Al_6(Si_6O_{18})(BO_3)_3(OH)_3F$.

4. Discussion

4.1 Cause of colour

Colours in tourmaline are essentially related to transitions elements (Ti, V, Cr, Fe, Mn and Cu), acting as colour-causing agents through several mechanisms at structural levels, with the most common ones being crystal field transitions (CFT), intervalence charge transfer (IVCT)

https://doi.org/10.1180/mgm.2024.42 Published online by Cambridge University Press

interactions, and colour centres (Fritsch and Rossman, 1987; Pezzotta and Laurs, 2011; Rossman, 2014). Since compositional analyses of the different coloured zones did not reveal V_2O_3 and Cr_2O_3 (values below the detection limit ≤0.03 wt%), the main transition metals that could contribute to the colour of the studied tourmaline grain are Fe, Mn, Ti and Cu.

The black colour characterising the core zone (C1, C2) hindered the recording of an optical absorption spectrum. Nevertheless, we can assess that such colour is mainly caused by the high absorbing Fe^{2+} transitions because of the abundance of this element in the inner core zone (FeO > 4 wt%).

The spectrum of the yellow intermediate zone (I1) shows a very strong absorption band in the near UV-region at ~30700 cm^{-1} and a sharp and very weak absorption band at ~24000 cm^{-1}, which can be assigned to Mn^{2+}-Ti^{4+} IVCT and Mn^{2+} spin-forbidden transitions, respectively (Rossman and Mattson, 1986; da Fonseca-Zang et al., 2008) (Figure 5). This assignment is consistent with the enrichment in MnO and TiO_2 observed from chemical data (Table 4). Because the yellow coloration is mainly caused by an intervalence charge transfer Mn^{2+}-Ti^{4+} interaction and to a minor extent by Mn^{2+} spin-forbidden transition, the I1 zone corresponds to the *canary* tourmaline gemmological variety described in Laurs et al. (2007).

The spectrum recorded in the pale blue-green intermediate zone (I2) reveals only the presence of a very weak broad band at ~14000 cm^{-1} and an intense broad band at ~11000 cm^{-1} in the near-infrared-range, both ascribed to Cu^{2+} spin-allowed *d-d* transitions (Rossman et al., 1991; Mashkovtsev et al., 2006) (Figure 5). EMPA results confirmed the enrichment in Cu in this part of the crystal, with an amount up to double than that of the yellow zone (Figure 3). This well fits with the different intensity of the absorption bands relative to Cu observed in the blue and the yellow zones. The relatively low MnO concentration (< 2 wt%) does not contribute to the colour through Mn^{2+} spin-forbidden electronic transitions, as Mn^{2+} is a weak absorber (Rossman, 2014). Additionally, the lack of TiO_2, does not allow Mn-Ti interaction and consequently the occurrence of a stronger Mn^{2+}-Ti^{4+} IVCT absorption band. Thus, in the absence of Fe (Table 4), Cu is the only

https://doi.org/10.1180/mgm.2024.42 Published online by Cambridge University Press

colour-causing agent for the pale blue-green coloration of the I2 zone. Moreover, based on overall results, the pale blue-green intermediate zone (I2) can be classified as *Paraiba* tourmaline variety (Laurs et al., 2008).

The recorded optical absorption spectrum of the purple intermediate zone (I3) is characterized by a weak and broad absorption band at ~22000 cm^{-1} and a stronger broad band at ~19000 cm^{-1}, both ascribable to Mn^{3+} *d-d* transitions (Reinitz and Rossman, 1988; Taran et al., 1993; Ertl et al., 2005; Bosi et al., 2017, 2021) (Figure 5 and Table 4). These assignments agree with the purple colour displayed by this part of the crystal, which can be ascribed to the presence of Mn^{3+} as colour-causing agent. On the basis of the intensity of the band at ~19000 cm^{-1} and using the molar extinction coefficient suggested by Reinitz and Rossman (1988), the Mn_2O_3 content was estimated to be 0.56 wt% (Table 1) in I3 zone. The origin of the broad and weak absorption bands at ~25200 cm^{-1} and ~14000 cm^{-1} is less obvious. The very low Fe- and Ti-content recorded by EMPA in this zone, rules out Fe^{2+}-Ti^{4+} IVCT as well as spin-allowed Fe^{2+} origins of these bands (Table 4). Other transition metals, such as Ni, can be taken into account (Taran et al., 1993), but the absence of Ni in this sample rules out this possibility. Thus, the origin of these two absorption bands remains unclear. According to these results, the purple coloration of the I3 zone is dominated by the presence of Mn in the oxidised trivalent state. Nevertheless, the relatively significant content of Cu could add a minor bluish hue to the colour. Hence, this variety of Cu-bearing rubellite may correspond to the gemmological variety *cuprian-rubellite* (Fritsch et al., 1990).

The spectrum of the dark-green prismatic overgrowth of the crystal displays two broad absorption bands centred at 13800 cm^{-1} and 9200 cm^{-1}, and a weak broad band at 24000 cm^{-1}, all attributable to the presence of relatively high level of Fe (FeO up to 1.4 wt%) (Figure 5). Mössbauer analysis shows, beside Fe^{3+}, also the presence of Fe^{2+}. Thus, the two strong bands at 13800 cm^{-1} and 9200 cm^{-1} can be caused by electronic exchange interactions between Fe^{2+}/Fe^{3+} pair at adjacent *Y* sites in the tourmaline structure (Taran and Rossman, 2002) (Table 4). The set of weak and relatively sharp bands between ~25000−24000 cm^{-1} can be instead assigned to spin-forbidden Fe^{2+}

https://doi.org/10.1180/mgm.2024.42 Published online by Cambridge University Press

and/or Fe^{3+} bands (Mattson and Rossman, 1987) (Table 4). In accord with these assignments, the dark-green coloration of the overgrowth is mainly controlled by Fe^{2+}/Fe^{3+} interactions.

4.2 Growth history

The analysed tourmaline sample is composed by a quite large detrital fragment, representing (from core-to-rim), all the growth sectors of an original crystal. Although there is no direct information about the primary deposit in which the original crystal formed, the changes of the chemical composition observed in the sample allows some significant inferences about the original growth stages as well as about the characteristics and the evolution of the crystallisation fluids.

The secondary Mavuco tourmaline deposit, where the studied sample has been collected, is located in the Alto Ligoña pegmatitic district, which is characterized by a crystalline basement of amphibolitic facies with migmatitic domes, in which a number of gem-bearing LCT pegmatites of the upper Neoproterozoic age have been intruded (Pinna et al., 1993; Bettencourt Dias and Wilson, 2000; Lächelt, 2004). The main features of the studied sample, as well as the minerals associated with tourmaline as residual grains in the secondary Mavuco deposit, clearly indicate a pegmatitic origin of the primary deposit. Thus, it represents, from core-to-rim, the stages of growth of an original tourmaline crystal of pegmatitic origin. Moreover, the relatively high gemmological quality and geochemical evolution of the studied tourmaline indicate that the original crystal formed in a core zone of a pegmatitic vein and, very likely, in a miarolitic cavity.

The black inner core of the crystal exhibits a significant enrichment in Fe and Mn (FeO > 5 wt% and MnO > 4 wt%). This enrichment is related to the amount of these elements available in the pegmatitic system during the early crystallisation of tourmaline. The subsequent progressive decrease in Fe, with FeO lowering down up to below the detection limit in the outermost part of the core zone, and remaining close to zero in the intermediate zone, is the result of its depletion in the system due mostly to tourmaline crystallization. MnO, indeed, shows an increase up to over 6 wt% in the intermediate zone, thus lowering down in the outermost intermediate zone to very low values

https://doi.org/10.1180/mgm.2024.42 Published online by Cambridge University Press

(< 0.5 wt%). The increased incorporation of Mn that characterises the yellow intermediate zone (I1) could be promoted by the depletion of Fe in the pegmatitic melt. In fact, the MnO content in the tourmaline crystal rises when FeO content starts to decrease (Figure 3), and this profile could be related to the behaviour of Mn during pegmatite crystallisation. Manganese is incompatible in typical magmatic primitive tourmaline (schorl-foitite), whereas Fe is very compatible, and thus the progressive increase in the Mn/Fe ratio of melt is driven by the crystallisation of tourmaline (London et al., 2001; Maner et al., 2019).

However, during the latest-stages of growth of the crystal, a sharp, new increase in Fe and Mn occurred, as documented by the dark-coloured prismatic overgrowth. A similar phenomenon has been described in the tourmaline crystals from Elba Island (Italy). These crystals are often characterised by a sudden late stage Fe and/or Mn enrichment, which results in a dark-coloured overgrowths, mostly evident at the termination of the crystals (Pezzotta, 2021; Altieri, 2023; Altieri et al., 2022, 2023a,b). As it has been argued for the Elba Island tourmalines petrogenetic model, a pocket rupture event related to brittle deformations occurring during the latest stages of crystallization of the cavities in the pegmatitic rock, was responsible for a partial opening of the geochemical system. According to this model, the highly reactive late-stage cavity fluids were able to penetrate into the fractures in the pegmatitic rock around the cavity. Consequently, this led to the hydrothermal alteration of the early- crystallised Fe- and Mn-rich minerals, such as Fe-rich micas and almandine-spessartine garnet. The release of Fe and Mn in the system caused a dramatic change in the chemical composition of the pocket environment with the subsequent formation of the dark-coloured overgrowth. The observed significant increase in Ca in the dark-coloured tourmaline overgrowth may be related to two potential factors. Firstly, it could be linked to the destabilisation of early crystallised plagioclase crystals in the pegmatitic rock. Alternatively, it could be the result of fluid contaminations coming from the metamorphic crystalline rocks in which the pegmatite was emplaced.

The CuO content is always confined to low levels, with the highest values (~0.15 wt%) in the I2

https://doi.org/10.1180/mgm.2024.42 Published online by Cambridge University Press

and the I3 zones. It is noteworthy that the highest values correspond to geochemically evolved growth sectors (Figure 3). The occurrence of Cu in pegmatitic systems is interpreted as a contamination of the pegmatitic liquids/fluids, which could be occurred at the source or even at the emplacement level (e.g., Beurlen et al., 2011; Beckett-Brown et al., 2023). However, the profile of the abundance of Cu in tourmaline crystals growth is still poorly documented.

The presence of Mn^{3+} in the I3 zone, which results in the pink-red coloration, could suggest a change towards oxidising conditions in the environment. This contrasts with the very low oxidising conditions in which the tourmaline crystallised. In fact, Mössbauer data show a Fe^{3+}/Fe_{tot} ratio of 0.02 in the core zone, the presence of only Fe^{2+} in the yellow intermediate zone (I1), and a Fe^{3+}/Fe_{tot} ratio of 0.04 that characterises the dark-green prismatic overgrowth. In this particular scenario, it proves challenging to elucidate the sudden and temporary transition to oxidised conditions in the environment during crystallisation of the observed pink-red I3 zone. The possibility of a geochemical system opening at this stage can be ruled out because no sudden changes in the chemical composition can be observed in the I3 zone. A possible explanation for the occurrence of Mn^{3+} in the I3 zone can be ascribed to the presence of a low amount of Mn^{3+} in the original melt. It has been reported that the Mn partition coefficients is anomalously low for Mn^{3+} and Mn uptake by tourmaline is dominated by Mn^{2+} (van Hinsberg, 2011). Thus, Mn^{3+}/Mn^{2+} ratio increased as consequence of the preferential incorporation of Mn^{2+} by tourmaline and the incorporation of Mn^{3+} occurred once Mn^{2+} has been completely depleted. Another explanation to account for the change in the redox state which occurred in the pink-red I3 zone, where Mn^{3+} prevails, is possible to assume that tourmaline, after crystallisation, encountered a natural radiation source, thereby inducing the Mn^{2+} oxidation and consequently leaving an overprint in the chemical composition. However, the oxidising effects of the radiation source became evident only in the I3 zone, characterised by the lowest Mn content and absence of Fe. We would suggest that, besides other phenomena, the Mn^{2+} and Ti^{4+} IVCT interaction may offer a stabilizing effect against the oxidation of Mn. According to this, the initial part of the crystal, up to the yellow intermediate zone (I1), is enriched in TiO_2 (> 0.4

https://doi.org/10.1180/mgm.2024.42 Published online by Cambridge University Press

wt%) and MnO (> 1.5 wt%), while TiO_2 is undetectable in the pink-red I3 zone. To the best of our knowledge, this explanation has not been proposed previously in the literature. It introduces a new concept that has the potential to open up a new area of research.

5. Conclusions

A fragment of a multicoloured tourmaline from the secondary deposit of Mavuco (Alto Ligoña, Mozambique), which represents the growth history from core-to-rim of the original crystal, has been studied. By combining data obtained from chemical and spectroscopic investigations, it was possible to determine the colour-causing agents that characterise the different coloured zones of the crystal.

The polychromatic feature of this tourmaline fragment highlights the petrogenetic potential of tourmaline as a powerful tool to register physicochemical variation in the crystallisation environment. However, the presence of a change in the redox state of Mn within a limited zone, probably occurred after the tourmaline crystallisation, may represent an evidence of a post-crystallisation alteration on the chemical signature of a tourmaline crystal.

Author Contributions: F.P. and F.B. conceived the project. F.B. created the working group. F.P. selected the research material and collected the field information. A.A. and F.B. provided EMPA data. H.S. and U.H. provided MS and OAS data. A.A. analyzed the data and wrote the first draft of the manuscript. F.P. contributed to the discussion section. All the authors reviewed the final version of the manuscript.

Funding: This research received funding by Sapienza University of Rome (Prog. Università 2023 to F.B.)

Acknowledgements: Sample preparation for chemical and spectroscopic analyses was carried out with the support of Dr. D. Mannetta to whom the authors express their gratitude. The authors

https://doi.org/10.1180/mgm.2024.42 Published online by Cambridge University Press

sincerely thank M. Serracino for his assistance during chemical analyses. The company Mozambique Mining is acknowledged for providing the studied sample. The authors sincerely thank the reviewers Peter Bačik and Andreas Ertl for their constructive comments that helped to improve the manuscript.

Conflict of Interest: The authors declare that there is no conflict of interest.

References

Altieri A. (2023) Definition of a genetic model for the dark-colored overgrowths in pegmatitic gem tourmaline crystals. *Plinius*, **49**, 23–29.

Altieri A., Pezzotta F., Skogby H., Hålenius U. and Bosi F. (2022) Blue-growth zones caused by Fe^{2+} in tourmaline crystals from the San Piero in Campo gem-bearing pegmatites, Elba Island, Italy. *Mineralogical Magazine*, **86**, 910–919.

Altieri A., Pezzotta F., Skogby H., Hålenius, U. and Bosi, F. (2023a) Dark-coloured Mn-rich overgrowths in an elbaitic tourmaline crystal from the Rosina pegmatite, San Piero in Campo, Elba Island, Italy: witness of late-stage opening of the geochemical system. *Mineralogical Magazine*, **87**, 130–142.

Altieri A., Pezzotta F., Andreozzi G.B., Skogby H., and Bosi F. (2023b) Genetic model for the color anomalies at the termination of pegmatitic gem tourmaline crystals from the island of Elba, Italy. *European Journal of Mineralogy*, **35**, 755–771.

Andreozzi G.B., Bosi F. and Longo M. (2008) Linking Mossbauer and structural parameters in elbaite-schorl-dravite tourmalines. *American Mineralogist*, **93**, 658–666.

Bosi F., Cámara F., Ciriotti M.E., Hålenius U., Reznitskii L. and Stagno V. (2017) Crystal-chemical relations and classification problems of tourma- lines belonging to the oxy-schorl–oxy-dravite–bosiite–povondraite series. *European Journal of Mineralogy*, **29**, 445–455.

Bosi F., Celata B., Skogby H., Hålenius U., Tempesta G., Ciriotti M.E., Bittarello E. and Marengo A. (2021) Mn-bearing purplish-red tourmaline from the Anjanabonoina pegmatite,

https://doi.org/10.1180/mgm.2024.42 Published online by Cambridge University Press

Madagascar. *Mineralogical Magazine*, **85**, 242–253.

Bosi F., Pezzotta F., Altieri A., Andreozzi G.B., Ballirano P., Tempesta G., Cempírek J., Škoda R., Filip J., Čopjacová R., Novák M., Kampf, A.R., Scribner E.D., Groat L.A. and Evans, R.J. (2022) Celleriite, $\square(Mn^{2+}{}_2Al)Al_6(Si_6O_{18})(BO_3)_3(OH)_3(OH)$, a new mineral species of the tourmaline supergroup. *American Mineralogist*, **107**, 31–42.

Beckett-Brown, C., McDonald, A.M. and McClenaghan, M.B. (2023) Trace element characteristics of tourmaline in porphyry Cu systems: development and application to discrimination. *The Canadian Journal of Mineralogy and Petrology,* **61**, 31–60.

Bettencourt Dias M., Wilson W.E. (2000) Famous mineral localities: The Alto Ligonha pegmatites, Mozambique. *Mineralogical Record*, **31**, pp. 459–497.

Beurlen, H., De Moura, O.J.M., Soares, D.R., Da Silva, M.R.R. and Rhede, D. (2011) Geochemical and geological controls on the genesis of gem-quality ‘‘Paraiba Tourmaline’’ in granitic pegmatites from northeastern Brazil. *The Canadian Mineralogist,* **49**, 277–300.

da Fonseca-Zang W.A, Zang J.W. and Hofmeister W. (2008) The Ti-Influence on the Tourmaline Color. *Journal of the Brazilian Chemical Society*, **19**, 1186–1192.

Dutrow B.L. and Henry D.J. (2011) Tourmaline: A geologic DVD. *Elements*, **7**, 301–306.

Dutrow B.L. and Henry D.J. (2018) Tourmaline compositions and textures: reflections of the fluid phase. *Journal of Geosciences*, **63**, 99–110.

Ertl A., Rossman G.R., Hughes J.M., Prowatke S. and Ludwig T. (2005) Mn-bearing “oxy-rossmanite” with tetrahedrally coordinated Al and B from Austria: Structure, chemistry and infrared and optical spectroscopic study. *American Mineralogist*, **90**, 481–487.

Ertl, A., Marschall, H.R., Giester, G., Henry, D.J., Schertl, H.-P., Ntaflos, T., Luvizotto, G.L., Nasdala, L., and Tillmanns, E. (2010): Metamorphic ultra high-pressure tourmalines: Structure, chemistry, and correlations to PT conditions. *American Mineralogist*, **95**, 1–10.

Ertl A., Giester G., Schüssler U., Brätz H., Okrusch M., Tillmanns E. and Bank H. (2013) Cu- and Mn-bearing tourmalines from Brazil and Mozambique: crystal structures, chemistry and

https://doi.org/10.1180/mgm.2024.42 Published online by Cambridge University Press

correlations. *Mineralogy and Petrology*, **107**, 265–279.

Fritsch E. and Rossman G.R. (1987) An update on color in gems. Part I. Introduction and colors caused by dispersed metal ions. *Gems and Gemology,* **23**, 126–139.

Fritsch E., Shigley J.E., Rossman G.R., Mercer M.E., Muhlmeister S.M. and Moon M. (1990) Gem-quality Cuprian-elbaite Tourmalines from São José Da Batalha, Paraíba, Brazil. *Gems and Gemology*, **26**, 189–205.

Henry D.J. and Dutrow B.L. (2018) Tourmaline studies through time: contributions to scientific advancements. *Journal of Geosciences*, **63**, 77–98.

Henry D.J., Novák M., Hawthorne F.C., Ertl A., Dutrow B., Uher P. and Pezzotta F. (2011) Nomenclature of the tourmaline supergroup minerals. *American Mineralogist*, **96**, 895–913.

Lächelt S. (2004) The Geology and Mineral Resources of Mozambique. National Directorate of Geology, Maputo, Mozambique, 515 pp.

Laurs B.M., Simmons W.B., Rossman G.R., Fritz E.A, Koivula J.I., Anckar B. and Falster A.U. (2007) Yellow Mn-rich tourmaline from the Canary Mining Area, Zambia. *Gems & Gemology*, **43**, 314–331.

Laurs B.M., Zwaan J.C., Breeding C.M., Simmons W.B., Beaton D., Rijsdijk K.F., Befi R. and Falster A.U. (2008) Copper-bearing (Paraiba-type) tourmaline from Mozambique. *Gems & Gemology*, **44**, 4–30.

London, D., Evensen, J.M., Fritz, E.A., Icenhower, J.P., Morgan, G.B. and Wolf, M.B. (2001) Enrichment and accomodation of manganese in granite-pegmatite systems. In Eleventh Annual V.M. Goldscmidt Conference p. abstract no. 3369. Hot Springs, Virginia.

Maner IV, J.L., London, D. and Icenhower, J.P. (2019) Enrichment of manganese to spessartine saturation in granite-pegmatite systems. *American Mineralogist*, **104**, 625–1637.

Mashkovtsev R.I., Smirnov S.Z. and Shigley J.E. (2006) The features of the Cu2+-entry into the structure of tourmaline. *Journal of Structural Chemistry*, **42**, 252–257.

Mattson S.M. and Rossman G.R. (1987) Fe^{2+}-Fe^{3+} interactions in tourmaline. *Physics and*

https://doi.org/10.1180/mgm.2024.42 Published online by Cambridge University Press

Chemistry of Minerals, **14**, 163–171.

Okrusch M., Ertl A., Schüssler U., Tillmanns E., Brätz H. And Bank H. (2016) Major- and trace-element composition of Paraíba-type Tourmaline from Brazil, Mozambique and Nigeria. *Journal of Gemmology*, **35**, 120–139.

Pesquera A., Gil-Crespo P.P., Torres-Ruiz F., Torres-Ruiz J. and Roda-Robles E. (2016) A multiple regression method for estimating Li in tourmaline from electron microprobe analyses. *Mineralogical Magazine*, **80**, 1129–1133.

Pezzotta F. (2021) A history of tourmaline from the Island of Elba. *The Mineralogical Record*, **52**, 669–720.

Pezzotta F. and Laurs B.M. (2011) Tourmaline: The kaleidoscopic gemstone. *Elements*, **7**, 331–336.

Pinna P., Jourde G., Calvez J.Y., Mroz J.P., Marques J.M. (1993) The Mozambique Belt in northern Mozambique: Neo-proterozoic (1100–850 Ma) crustal growth and tectogenesis, and superimposed Pan-African (800–550 Ma) tectonism. *Precambrian Research*, **62**, pp. 1–59.

Pouchou J.L. and Pichoir F. (1991) Quantitative analysis of homogeneous or stratified microvolumes applying the model "PAP". Pp. 31–75 in: Electron Probe Quantitation (K.F.J. Heinrich and D.E. Newbury, editors). Plenum, New York.

Prescher C., McCammon C. and Dubrowinsky L. (2012) MossA: a program for analyzing energy-domain Mössbauer spectra from conventional and synchrotron sources. *Journal of Applied Crystallography*, **45**, 329–331.

Reinitz I. and Rossman G.R. (1988) Role of natural radiation in tourmaline coloration. *American Mineralogist*, **73**, 822–825.

Rossman G.R. (2014) Optical spectroscopy. In: Henderson G.S., Neuville D.R., Downs R.T. (eds) Spectroscopy Methods in Mineralogy and Materials Sciences. Reviews in Mineralogy and Geochemistry, **78**, 371–398.

Rossman G.R. and Mattson S.M. (1986) Yellow, Mn-rich elbaite with Mn-Ti intervalence charge transfer. *American Mineralogist*, **71**, 599–602.

https://doi.org/10.1180/mgm.2024.42 Published online by Cambridge University Press

Rossman G.R., Fritsch E. and Shigley J.E. (1991) Origin of color in cuprian elbaite from São José de Batalha, Paraíba, Brazil. *American Mineralogist*, **76**, 1479–1484.

Taran M.N and Rossman G.R. (2002) High-temperature, high-pressure optical spectroscopic study of ferric-iron-bearing tourmaline. *American Mineralogist*, **87**, 1148–1153.

Taran M.N., Lebedev, A.S. and Platonov A.N. (1993) Optical absorption apectroscopy of synthetic tourmalines. *Physics and Chemistry of Minerals*, **20**, 209–220.

van Hinsberg V.J. (2011) Preliminary experimental data on trace-element partitioning between tourmaline and silicate melt. *The Canadian Mineralogist*, **49**, 153–163.

van Hinsberg V.J., Henry D.J. and Dutrow B.L. (2011a) Tourmaline as a petrologic forensic mineral: A unique recorder of its geologic past. *Elements*, **7**, 327–332.

van Hinsberg V.J., Henry D.J. and Marschall H.R. (2011b) Tourmaline: an ideal indicator of its host environment. *The Canadian Mineralogist*, **49**, 1–16.

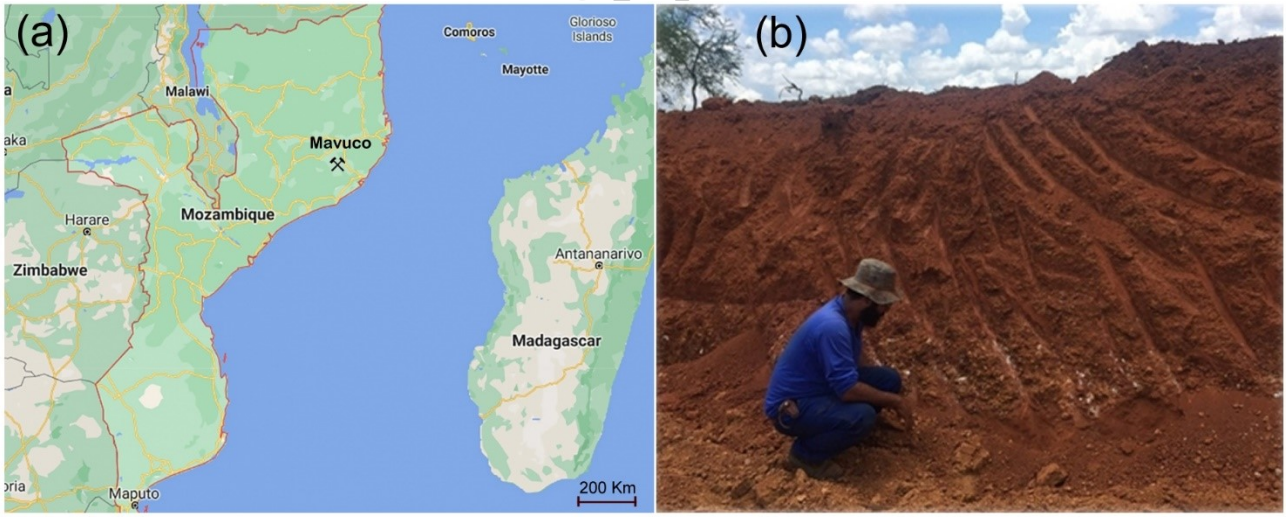

Figure 1. a) The occurrence area of the analyzed tourmaline sample is marked in the eastern portion of the Pegmatitic District of Alto Ligoña, NE Mozambique; b) Cross-section of the soil of the secondary deposit of Mavuco. Tourmalines are found in a light reddish-brown quartz-rich gravel layer (locally called *kamada*) on top of a light tan weathered bedrock, and underneath a layer of red-brown clayey-bauxitic soil (locally called *kororo*). Photo by F. Pezzotta.

https://doi.org/10.1180/mgm.2024.42 Published online by Cambridge University Press

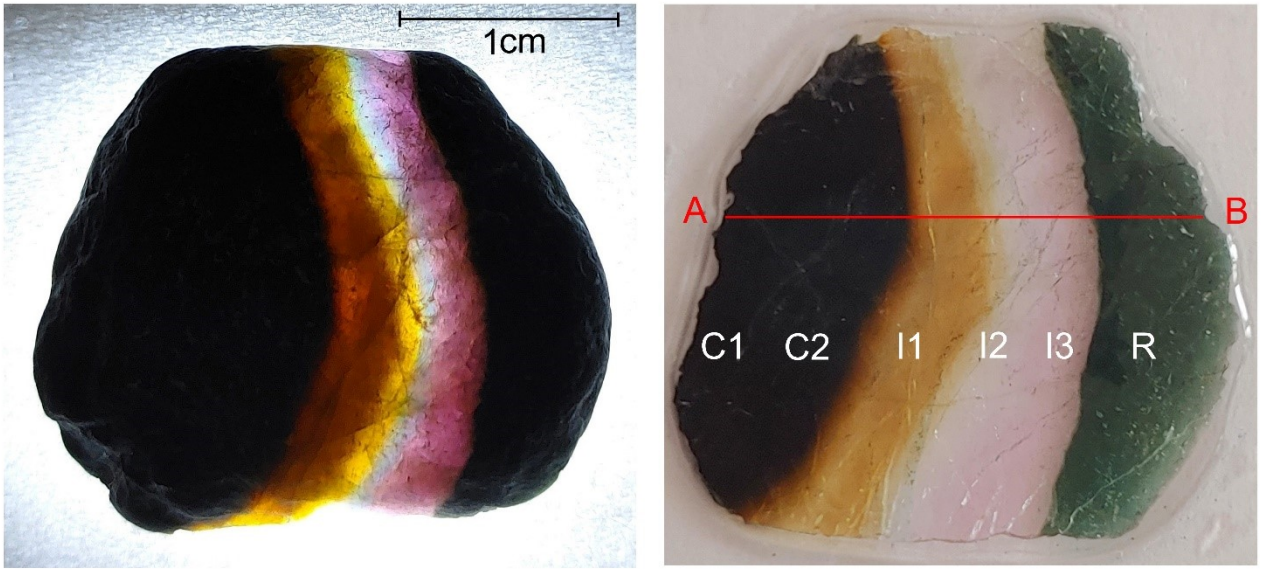

Figure 2. The polychromatic tourmaline sample analyzed in this work (image to the left) and the corresponding thin (500 μm) section (image to the right). Sample size: 2.5 cm. Sample weight: 12.75 gr. Scale bar = 1 cm. The analyzed traverse (A-B) is represented by a solid red line. Based on colour/chemistry, the different coloured zones were labelled: C1, C2 = core zones; I1= yellow intermediate zone, I2 = pale blue-green intermediate zone (note that the real colour of the crystal in the figure is only broadly visible because of backlighting, which is fading the real colour) and I3 = pink-red intermediate zone; R = prismatic overgrowth.

https://doi.org/10.1180/mgm.2024.42 Published online by Cambridge University Press

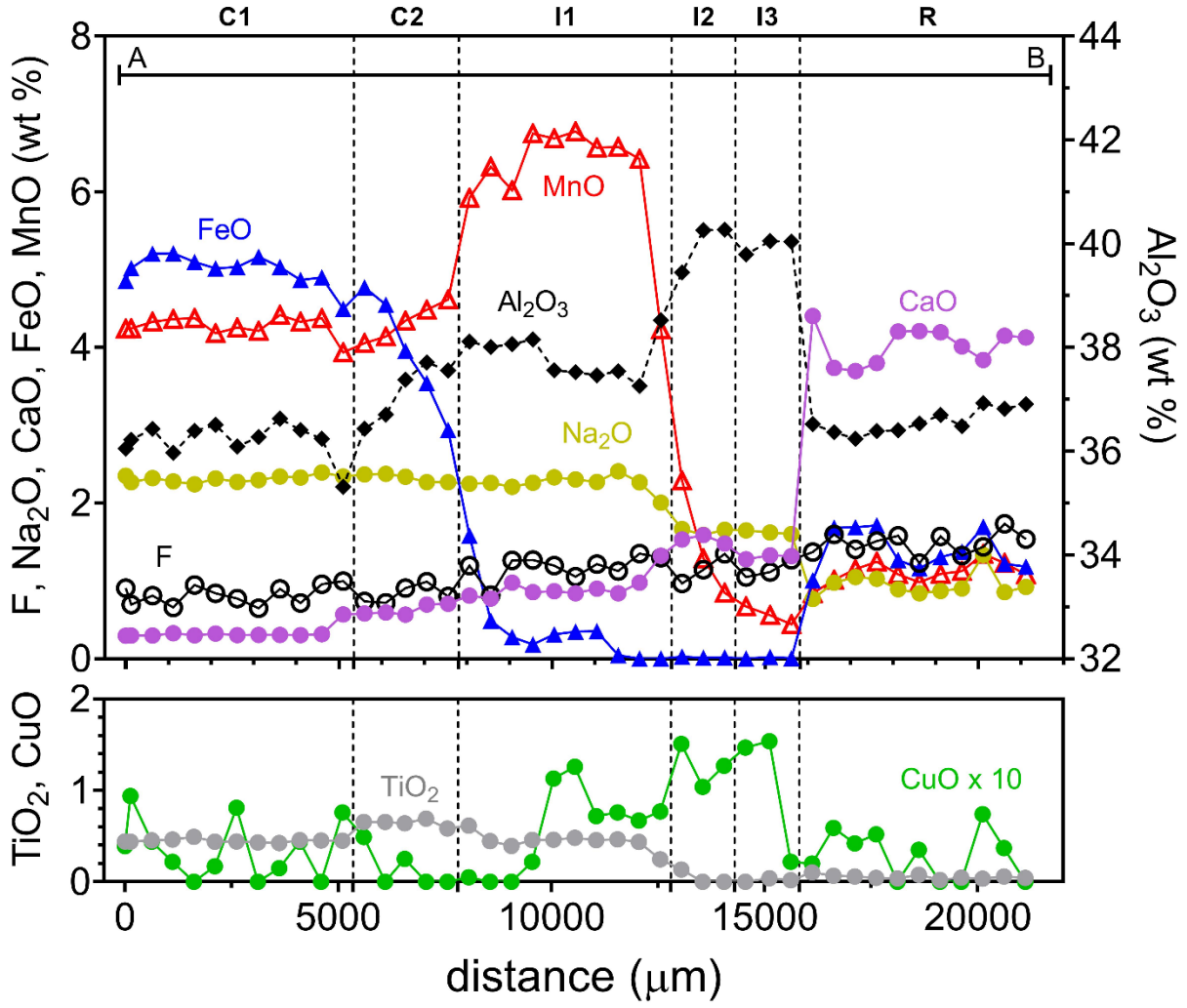

Figure 3. Results of EMP analysis of the tourmaline sample (only selected oxides are reported). See Table 1 for complete chemistry.

https://doi.org/10.1180/mgm.2024.42 Published online by Cambridge University Press

(a)

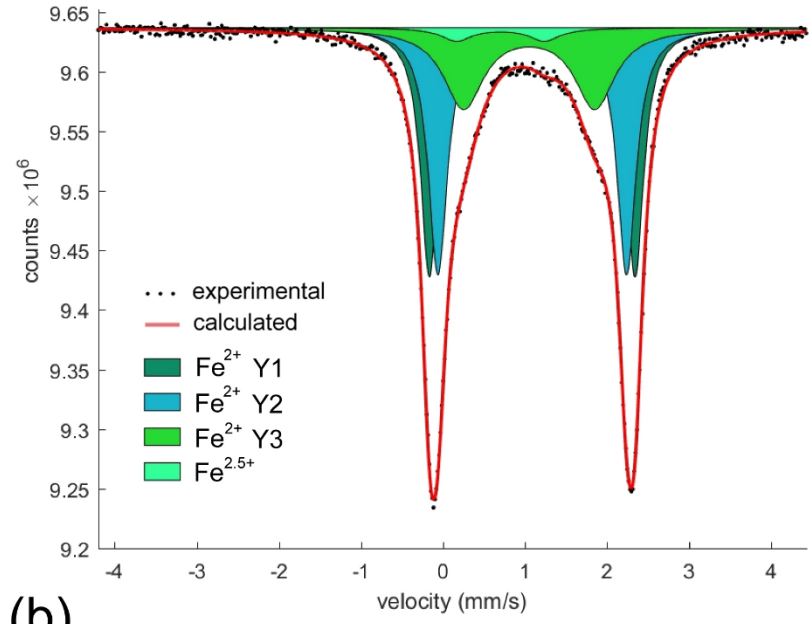

(b)

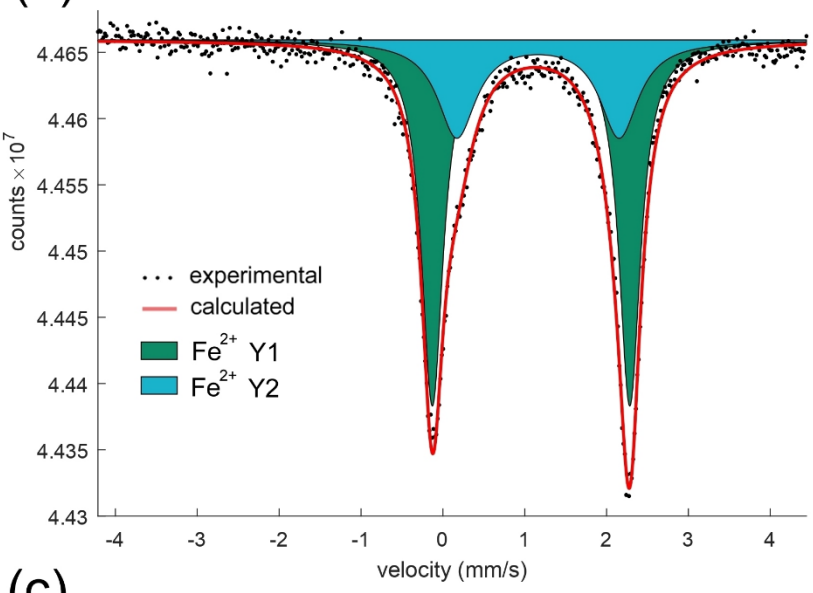

(c)

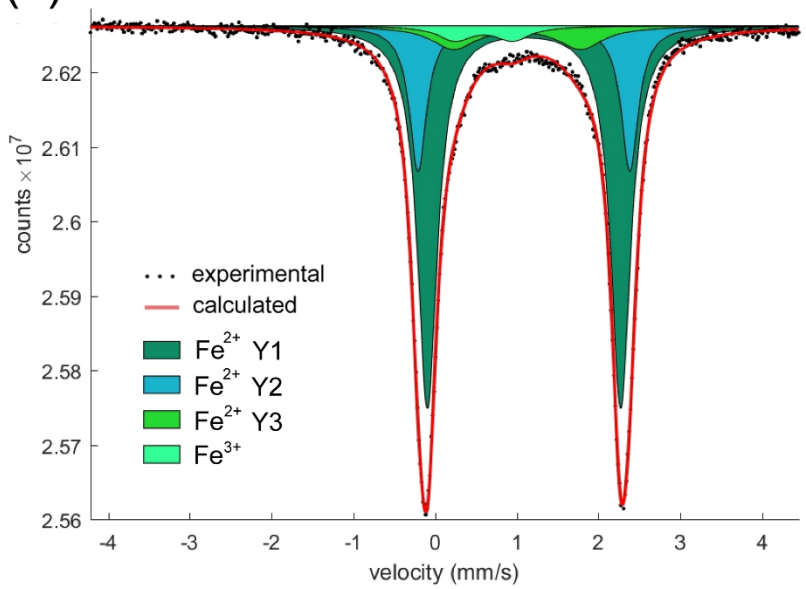

https://doi.org/10.1180/mgm.2024.42 Published online by Cambridge University Press

Figure 4. Room temperature ^{57}Fe Mössbauer spectra for the black core (C1, C2), the yellow intermediate zone (I1) and the dark-green prismatic rim (R). For all the coloured zones (a, b, c), experimental spectrum (exp) is represented by dots, and calculated spectrum (calc) by thick red curve. Lorentzian absorption doublets assigned to $^{[6]}Fe^{2+}$ are represented by dark-green, light blue and light green coloured areas. The neon-green coloured area refers to the assignment of $^{[6]}Fe^{2.5+}$ and $^{[6]}Fe^{3+}$.

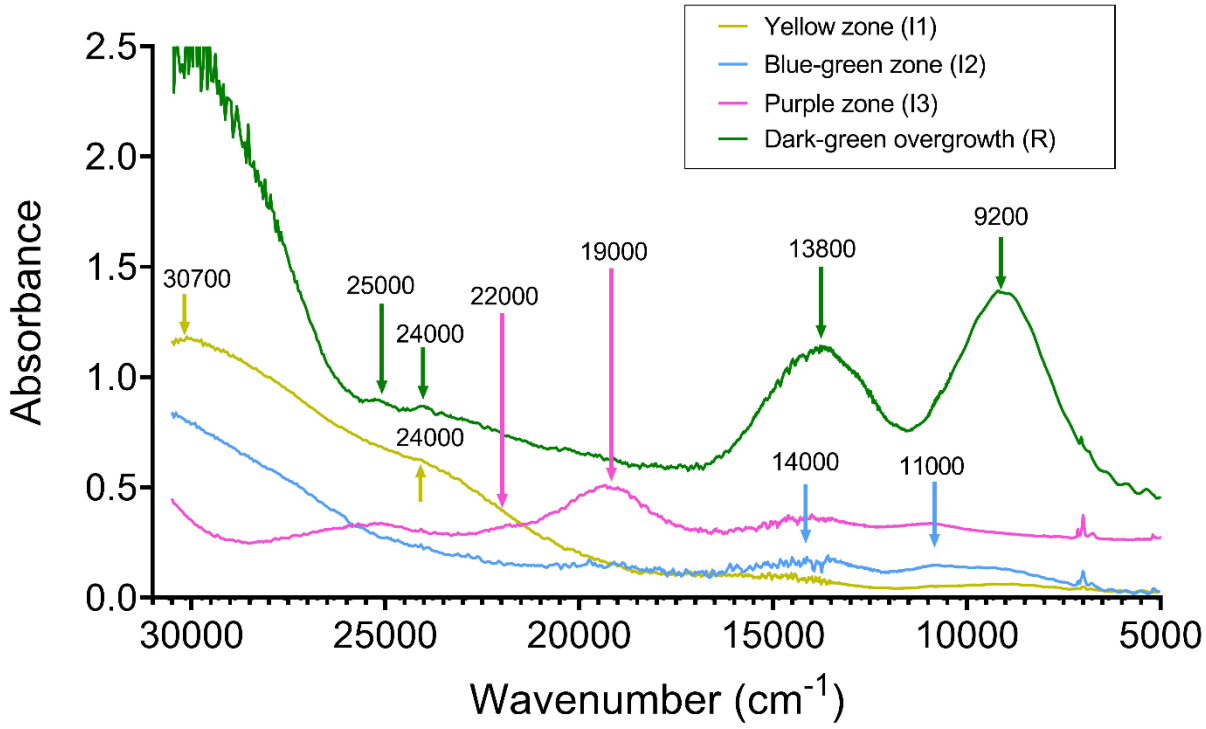

Figure 5. Optical absorption spectra for the different coloured zones of the analyzed tourmaline sample. Sample thickness: yellow intermediate zone = 280 µm; pale blue-green intermediate zone: 838 µm; purple intermediate zone: 843 µm; dark-green overgrowth: 424 µm. The main absorption bands are indicated.

https://doi.org/10.1180/mgm.2024.42 Published online by Cambridge University Press

Table 1. Average chemical composition from EMPA and atoms per formula unit (apfu) for the different coloured zones of the tourmaline sample studied (Mavuco area, Alto Ligoña pegmatite district, NE Mozambique).

	C1	**C2**	**I1**	**I2**	**I3**	**R**
	n = 12	*n* = 5	*n* = 10	*n* = 3	*n* = 3	*n* = 11
SiO_2 (wt%)	37.16(27)	36.45(16)	37.55(54)	38.86(29)	39.64(2)	39.40(25)
TiO_2	0.45(2)	0.65(4)	0.45(9)	0.04(8)	0.02(2)	0.05(2)
B_2O_3[a]	10.66	10.62	10.83	11.09	11.15	10.95
Al_2O_3	36.21(34)	37.16(56)	37.82(40)	39.99(47)	39.96(15)	36.57(23)
FeO	4.99(20)	3.95(75)	0.36(46)	0.02(1)	0.01(1)	1.39(26)
Fe_2O_3[c]	0.09	-	-	-	-	0.06
MnO	4.27(13)	4.33(23)	6.23(76)	1.47(74)	0.06(11)	1.11(14)
Mn_2O_3[d]	-	-	-	-	0.56	-
MgO	0.03(1)	0.01(1)	0.00(1)	0.01(1)	-	0.19(6)
CuO	0.04(3)	0.01(2)	0.06(5)	0.13(2)	0.11(7)	0.03(3)

This is a 'preproof' accepted article for Mineralogical Magazine. This version may be subject to change during the production process.
DOI: 10.1180/mgm.2024.42

CaO	0.33(8)	0.63(7)	0.92(16)	1.53(5)	1.31(3)	4.03(23)
Na_2O	2.31(4)	2.32(5)	2.26(10)	1.64(4)	1.62(2)	0.95(15)
Li_2O [b]	1.00	0.97	1.36	2.09	2.34	2.39
K_2O	0.03(1)	0.03(1)	0.02(1)	0.01(1)	0.02(1)	0.01(1)
F	0.82(12)	0.83(12)	1.18(15)	1.15(19)	1.14(11)	1.48(14)
H_2O[a]	2.91	2.71	2.74	2.98	2.93	2.61
–O ≡ F	−0.35	−0.35	−0.50	−0.49	−0.48	−0.62
Total	100.92	100.35	101.29	100.53	100.32	100.51
Atoms normalized to 31 anions						
Si (apfu)	6.057	5.968	6.023	6.091	6.179	6.185
Ti^{4+}	0.055	0.079	0.054	0.005	0.002	0.006
B	3.000	3.000	3.000	3.000	3.000	3.000
Al	6.955	7.170	7.151	7.388	7.342	6.889
Fe^{2+}	0.669	0.541	0.048	0.002	0.001	0.175
Fe^{3+}	0.011	-	-	-	-	0.008
Mn^{2+}	0.590	0.600	0.846	0.196	0.008	0.147
Mn^{3+}	-	-	-	-	0.066	-
Mg	0.007	0.002	0.000	-	-	0.047
Cu	0.005	0.001	0.007	0.014	0.013	0.004

https://doi.org/10.1180/mgm.2024.42 Published online by Cambridge University Press

Ca	0.057	0.110	0.157	0.258	0.218	0.679
Na	0.731	0.738	0.702	0.498	0.491	0.289
Li	0.655	0.639	0.878	1.318	1.467	1.509
K	0.006	0.007	0.005	0.003	0.003	0.003
F	0.423	0.430	0.598	0.571	0.564	0.736
OH	3.170	2.965	2.930	3.118	3.042	3.264

[a] Calculated by stoichiometry (see text)
[b] Estimated with the procedure of Pesquera et al. (2016)
[c] Calculated by Mössbauer analysis; for C1 and R, FeO_{EMPA} = 4.99(20) wt% and FeO_{EMPA} = 1.39(26) wt%, respectively
[d] Determined by OAS spectroscopy
Errors for oxides and fluorine are standard deviations (in brackets)

Table 2. Room temperature ^{57}Fe Mössbauer parameters for the FeO-rich coloured zones of the tourmaline sample investigated in this study.

	δ mm/s	**ΔE_Q mm/s**	**Γ mm/s**	**Assignment**	**%Area**
Black core (C1, C2)	1.09	2.51	0.26	Fe^{2+} (*Y*1)	35
	1.09	2.30	0.28	Fe^{2+} (*Y*2)	37
	1.05	1.60	0.59	Fe^{2+} (*Y*3)	25
	0.70	1.07	0.47	$Fe^{2.5+}$	3
Yellow zone (I1)	1.08	2.41	0.32	Fe^{2+} (*Y*1)	68
	1.16	1.98	0.57	Fe^{2+} (*Y*2)	32

https://doi.org/10.1180/mgm.2024.42 Published online by Cambridge University Press

	1.09	2.37	0.30	Fe^{2+} (*Y*1)	66
Dark-green overgrowth (R)	1.09	2.59	0.25	Fe^{2+} (*Y*2)	21
	1.01	1.56	0.66	Fe^{2+} (*Y*3)	9
	0.60	0.71	0.50	Fe^{3+}	4

Centroid shift (δ) in mm/s relative to α-Fe foil; errors are estimated no less than ±0.02 mm/s for δ, quadrupole splitting (ΔE_Q), and peak width (Γ), and no less than ±3% for doublets areas.

Table 3. Empirical formulae for the different coloured zones of the tourmaline sample investigated in this study.

Coloured zones	Empirical formulae
Black inner core (C1)	$^{X}(Na_{0.73}K_{0.01}\square_{0.21}Ca_{0.06})_{\Sigma 1.00}{}^{Y}(Al_{0.96}Li_{0.66}Fe^{2+}_{0.67}Fe^{3+}_{0.01}Mn^{2+}_{0.59}Mg_{0.01}Ti_{0.06})_{\Sigma 2.94}{}^{Z}Al_6(^{T}Si_{6.06}O_{18})(BO_3)_3{}^{V}(OH)_{3.00}{}^{W}(OH_{0.17}F_{0.42}O_{0.41})_{\Sigma 1.00}$
Black outer core (C2)	$^{X}(Na_{0.74}K_{0.01}\square_{0.14}Ca_{0.11})_{\Sigma 1.00}{}^{Y}(Al_{1.14}Li_{0.64}Fe^{2+}_{0.54}Mn^{2+}_{0.60}Ti_{0.08})_{\Sigma 3.00}{}^{Z}Al_6[(^{T}Si_{5.97}Al_{0.03})O_{18}](BO_3)_3{}^{V}(OH_{2.97}O_{0.03})_{\Sigma 3.00}{}^{W}(F_{0.43}O_{0.57})_{\Sigma 1.00}$
Yellow intermediate zone (I1)	$^{X}(Na_{0.70}\square_{0.14}Ca_{0.16})_{\Sigma 1.00}{}^{Y}(Al_{1.15}Li_{0.88}Fe^{2+}_{0.05}Mn^{2+}_{0.85}Cu_{0.01}Ti_{0.05})_{\Sigma 2.99}{}^{Z}Al_6(^{T}Si_{6.01}O_{18})(BO_3)_3{}^{V}(OH_{2.93}O_{0.07})_{\Sigma 3.00}{}^{W}(F_{0.60}O_{0.40})_{\Sigma 1.00}$
Blue-green intermediate zone (I2)	$^{X}(Na_{0.50}\square_{0.24}Ca_{0.26})_{\Sigma 1.00}{}^{Y}(Al_{1.39}Li_{1.32}Mn^{2+}_{0.20}Cu_{0.01})_{\Sigma 2.91}{}^{Z}Al_6(^{T}Si_{6.09}O_{18})(BO_3)_3{}^{V}(OH)_{3.00}{}^{W}(OH_{0.12}F_{0.57}O_{0.31})_{\Sigma 1.00}$
Purple intermediate zone (I3)	$^{X}(Na_{0.49}\square_{0.29}Ca_{0.22})_{\Sigma 1.00}{}^{Y}(Al_{1.34}Li_{1.47}Mn^{3+}_{0.07}Mn^{2+}_{0.01}Cu_{0.01})_{\Sigma 2.90}{}^{Z}Al_6(^{T}Si_{6.18}O_{18})(BO_3)_3{}^{V}(OH)_{3.00}{}^{W}(OH_{0.04}F_{0.57}O_{0.39})_{\Sigma 1.00}$
Dark-green prismatic overgrowth (R)	$^{X}(Na_{0.29}\square_{0.03}Ca_{0.68})_{\Sigma 1.00}{}^{Y}(Al_{0.89}Li_{1.51}Fe^{2+}_{0.18}Fe^{3+}_{0.01}Mn^{2+}_{0.15}Mg_{0.05}Ti_{0.01})_{\Sigma 2.80}{}^{Z}Al_6(^{T}Si_{6.19}O_{18})(BO_3)_3{}^{V}(OH)_{3.00}{}^{W}(OH_{0.26}F_{0.74})_{\Sigma 1.00}$

https://doi.org/10.1180/mgm.2024.42 Published online by Cambridge University Press

Table 4. Interpretation of OAS results for selected spots on the different coloured zones displayed by the tourmaline sample studied.

Colour	FeO (wt%)	MnO (wt%)	TiO_2 (wt%)	CuO (wt%)	Absorption bands	Assignments
Yellow intermediate zone (I1)	-	6.42	0.44	0.07	~30700 cm^{-1}	Mn^{2+}-Ti^{4+} IVCT transitions
					~24000 cm^{-1}	Mn^{2+} spin-forbidden transitions
Blue-green intermediate zone (I2)	0.02	1.47	0.04	0.13	~14000 cm^{-1}	Cu^{2+} *d-d* transitions
					~11000 cm^{-1}	Cu^{2+} *d-d* transitions
Purple intermediate zone (I3)	0.01	0.56	0.02	0.02	~22000 cm^{-1}	Mn^{3+} *d-d* transitions
					~19000 cm^{-1}	Mn^{3+} *d-d* transitions
Dark-green prismatic overgrowth (R)	1.37	1.20	0.05	0.03	~25000 cm^{-1}	Fe^{2+} and/or Fe^{3+} spin-forbidden transitions
					~24000 cm^{-1}	Fe^{2+} and/or Fe^{3+} spin-forbidden transitions
					~13800 cm^{-1}	Fe^{3+}-Fe^{2+} exchange-coupled pairs
					~9200 cm^{-1}	Fe^{3+}-Fe^{2+} exchange-coupled pairs

https://doi.org/10.1180/mgm.2024.42 Published online by Cambridge University Press